Multibeam Design for Joint Communication and Sensing in 5G New Radio Networks

Carlos Baquero Barneto, Sahan Damith Liyanaarachchi, Taneli Riihonen, Lauri Anttila, and Mikko Valkama
Electrical Engineering, Faculty of Information Technology and Communication Sciences, Tampere University, Finland
carlos.baquerobarneto@tuni.fi

***Abstract*—The large available bandwidths at millimeter-wave (mmW) frequencies enable very high data rates and reduced latencies while can also facilitate high-resolution radio-based sensing. In this paper, we address the problem of providing the communications and sensing functionalities simultaneously at the same frequencies, with specific emphasis on the emerging 5G New Radio (NR) networks. To this end, a novel RF beamforming design and optimization approach is proposed, for dual-functional joint radar-communication systems, providing multiple simultaneous transmit beams to support efficient beamformed communications while an additional beam simultaneously senses the environment around the base-station. The proposed beamforming approach jointly optimizes the transmitter and receiver beamforming weights in order to maximize the sensing performance and mitigate the possible interference stemming from the communication beam, while guaranteeing also the target beamforming gain for the communications link. The performance of the proposed approach is assessed through comprehensive numerical evaluations, demonstrating that substantial gains and benefits can be achieved compared to more ordinary beamforming approaches.**

***Index Terms*—5G New Radio (NR), millimeter waves, RF beamforming, joint communications and sensing, multibeam, radar, RF convergence.**

I. Introduction

Wireless communication networks are evolving to provide larger capacities and reduced latencies, while at the same time various radio-based sensing schemes are receiving increasing interest in both civilian and professional applications [1], [2]. As a result, the radio spectrum congestion is becoming increasing critical, which in turn is catalyzing two interesting research directions under the so-called RF convergence paradigm. First direction is dealing with the radar-communication coexistence (RCC) scenarios [1], where the communication and radar systems operate simultaneously but treat each other as independent interferers. The second and more challenging approach focuses on designing joint communication and sensing (JCAS) systems that can perform both functionalities sharing the same transmit signals and potentially the same hardware platforms [3], [4]. Some relevant applications where JCAS systems can play an important role are autonomous vehicle networks, unmanned aerial vehicle (UAV) control systems, building analytics and digital health monitoring [5], [6].

This work was partially supported by the Academy of Finland (grants #310991, #315858, and #328214), Nokia Bell Labs, and the Doctoral School of Tampere University. The work was also supported by the Finnish Funding Agency for Innovation under the "RF Convergence" project.

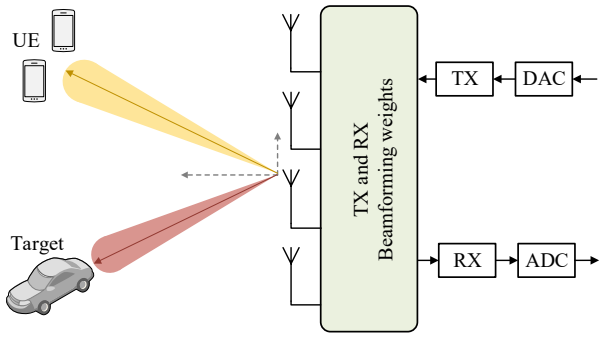

Fig. 1. Considered scenario and system model for multibeam-based joint communications and sensing/radar in mmW 5G NR network. A single phased-array shared between TX and RX is considered in this work.

The emerging 5G NR networks aim to provide large improvements in terms of peak data rates, latency, reliability and network capacity [7], compared to earlier mobile network generations. As a consequence, new operating bands have been defined, including also selected mmW bands that facilitate large channel bandwidths up to 400 MHz. Such large bandwidths enable also highly-accurate time-based measurements and hence high resolution for radar operation [3], [8], [9].

At mmW frequencies, active antenna arrays and steerable beams need to be used to overcome large propagation losses. Existing research in JCAS context mostly focuses on single-beam approaches per phased-array, however, this approach essentially limits the sensing direction to be the same as that of the communication node [6], [10]. To overcome this problem, selected recent studies have raised the idea of using separate simultaneous beams for communication and sensing functionalities. To this end, in [11], a multibeam framework and a beamforming design with two analog arrays are proposed to simultaneously support communication and sensing. The beamforming design considers different requirements, where sensing requires time-varying directional beams to sense the environment, while communication requires stable and accurately-aimed beams to achieve a good link quality. In [8], a multibeam algorithm provides coherent beam in the transmitter antenna array towards the communication node while simultaneously perturbing the sidelobes. Sidelobe perturbation results in random beams with low antenna gain, which are exploited for short-range radar applications.

In JCAS systems, developing efficient interference manage-

ment techniques is essential, so that the communication and sensing can operate simultaneously without interfering each other. Similarly, in the proposed system presented in Fig. 1 where the 5G base-station, referred to as gNB, operates as a dual-functional radar-communication node using multiple beams, the reflections from the direction of the communication beam act as interference from the sensing perspective. In this paper, we propose to improve the sensing performance of 5G NR networks through novel beamforming optimization approach, that minimizes the communication beam interference while also simultaneously ensuring a certain beamformed communications quality. Additionally, the proposed approach allows for flexibly configuring the sensing beam direction, independent of the communications direction.

The rest of the paper is organized as follows: In Section II, the considered system model is shortly presented. Then, in Section III, the proposed beamformer optimization formulation is described. In Section IV, extensive numerical results are provided and analyzed to assess the proposed multibeam optimization approach and achievable performance. Finally, Section V concludes our work.

II. System Model

In this work, similar to [12], we assume that the radar functionality is performed in the base-station unit (gNB) of a 5G NR network, by utilizing the known downlink transmit waveform $s(t)$. We pursue a new functionality that enables the gNB to simultaneously sense the environment with a directive and configurable beam while another directive beam is dedicated for the communications link as illustrated in Fig. 1. Additionally, we consider planar wavefront and assume a single shared uniform linear array (ULA) for TX and RX with N antenna elements uniformly spaced at half the wavelength, and assume separate RF beamforming weights for TX and RX.

As is well-known [13], the array response of the gNB phased-array reads

$$\mathbf{a}(\theta) = \left[1, e^{j\pi \sin(\theta)}, \ldots, e^{j\pi(M-1)\sin(\theta)}\right]^T, \quad (1)$$

where θ refers to either the angle of departure (AoD), θ_{tx}, or the angle of arrival (AoA), θ_{rx}. The radiated spatial waveform $\mathbf{x}(t)$ can then be expressed as

$$\mathbf{x}(t) = s(t)\mathbf{w}_{\text{tx}}, \quad (2)$$

where $\mathbf{w}_{\text{tx}}$ denotes the TX beamforming vector. The radiated spatial waveform $\mathbf{x}(t)$ then propagates over-the-air and interacts with one or multiple targets, producing reflections that will be collected by the gNB receiving system [14] for sensing/radar purposes. With K targets, the receive spatial waveform can be described by

$$\mathbf{y}(t) = \sum_{k=0}^{K-1} b_k e^{2\pi j f_{\text{D},k} t} \mathbf{a}(\theta_{\text{rx},k}) \mathbf{a}^T(\theta_{\text{tx},k}) \mathbf{x}(t-\tau_k) + \mathbf{n}(t), \quad (3)$$

where the relative delay and Doppler shift of the kth target correspond to τ_k and $f_{\text{D},k}$, respectively, while b_k models the attenuation factor of the kth reflection. The noise vector is denoted by $\mathbf{n}(t)$. It is noted that perfect isolation between the TX and RX systems is assumed in this work, for simplicity, while practical methods to facilitate feasible isolation are described in [12]. Similar to (2), beamforming is then applied in the receiver side, combining all the signals from each array element which is expressed as

$$y(t) = \mathbf{w}_{\text{rx}}^T \mathbf{y}(t). \quad (4)$$

Targets are detected based on the comparison between the TX waveform $s(t)$ and the beamformed RX waveform $y(t)$. The classical approach for range estimation is the matched filter (MF) processing [13], which maximizes the signal-to-noise ratio (SNR) of the received reflections. It is noted that more efficient and specific techniques for OFDM radar, based on the frequency-domain processing, can also be applied [6], [12].

In general, the TX and RX beamforming weights are subject to specific constraints depending on the hardware architecture. For clarity, the RF beamforming vectors are expressed as

$$\begin{aligned} \mathbf{w}_{\text{tx}} &= \left[\alpha_{\text{tx},0} e^{j\beta_{\text{tx},0}}, \ldots, \alpha_{\text{tx},N-1} e^{j\beta_{\text{tx},N-1}}\right]^T, \\ \mathbf{w}_{\text{rx}} &= \left[\alpha_{\text{rx},0} e^{j\beta_{\text{rx},0}}, \ldots, \alpha_{\text{rx},N-1} e^{j\beta_{\text{rx},N-1}}\right]^T, \end{aligned} \quad (5)$$

where $\alpha_{\text{tx},n} = (\boldsymbol{\alpha}_{\text{tx}})_n$ and $\alpha_{\text{rx},n} = (\boldsymbol{\alpha}_{\text{rx}})_n$ correspond to the TX and RX amplitude weights of the nth antenna element, respectively. Similarly, $\beta_{\text{tx},n} = (\boldsymbol{\beta}_{\text{tx}})_n$ and $\beta_{\text{rx},n} = (\boldsymbol{\beta}_{\text{rx}})_n$ denote the TX and RX phase shifts at the nth antenna. In this article, in the JCAS beamforming optimization, we consider the following three scenarios and corresponding beamforming related hardware architectures:

- First, an array architecture (Arch.1) that allows only for the phase control of TX and RX elements is considered, implying that the amplitudes $\alpha_{\text{tx},n}$ and $\alpha_{\text{rx},n}$ are mutually identical and constant for all n. This reflects ordinary phased-array processing.
- Then, a second architecture (Arch.2) with only phase control in TX but allowing both amplitude and phase control in RX is considered. In this case, only the TX amplitudes $\alpha_{\text{tx},n}$ are constant for all n.
- Finally, we also consider the most flexible array architecture (Arch.3) allowing full amplitude and phase control of all the TX and RX elements, without any constraints.

III. Proposed JCAS Beamformer Optimization

We next propose and formulate a joint optimization framework for the transmitter and receiver beamforming vectors $\mathbf{w}_{\text{tx}}$ and $\mathbf{w}_{\text{rx}}$, such that the selected beamformed communications requirements are met, while maximizing the ability to simultaneously sense targets in another direction. For this purpose, we quantify the effect of the beamforming vectors $\mathbf{w}_{\text{tx}}$ and $\mathbf{w}_{\text{rx}}$ in the communications and radar performance by using the array factors. In general, according to the 5G NR radio interface numerology [7], the antenna arrays operating at mmW carrier frequencies at or above 28 GHz with transmission bandwidths up to 400 MHz provide fractional bandwidths (FBWs) of less than 1.5%, therefore, we can assume and consider narrowband array models in the continuation.

A. Array Factors and Reference Solution

Considering the radiated or incident signal from a plane wave at an angle θ, the TX or RX array factor of an N-element ULA with weights $\alpha_n e^{j\beta_n}$ can be expressed as [13]

$$F(\theta) = \sum_{n=0}^{N-1} \alpha_n e^{j\frac{2\pi d n}{\lambda}\sin(\theta)+j\beta_n}, \tag{6}$$

where d and λ correspond to the antenna element separation and the signal wavelength, respectively. Furthermore, the *combined radar pattern* (CRP) which refers to the equivalent radiation pattern for the radar system, can be expressed by the multiplication of both the TX and RX radiation patterns, as

$$|R_{\text{rad}}(\theta)|^2 = |F_{\text{tx}}(\theta)|^2 \, |F_{\text{rx}}(\theta)|^2 . \tag{7}$$

Assuming that the considered JCAS system provides a communication link at an angle of θ_{com} while simultaneously senses a target at another angle of θ_{rad}, beamforming optimization could be applied in TX and RX separately [15]. In the TX side, beamforming weights can be optimized to provide multiple beams [11], one for communications and another one for sensing, while the receiver only provides a beam for radar. To design the TX beamformer, the matrix $\mathbf{A}_{\text{tx}}$ containing the steering vectors of the two desired beam directions can be expressed as

$$\mathbf{A}_{\text{tx}} = \begin{bmatrix} 1 & 1 \\ e^{j\frac{2\pi d}{\lambda}\sin(\theta_{\text{com}})} & e^{j\frac{2\pi d}{\lambda}\sin(\theta_{\text{rad}})} \\ \vdots & \vdots \\ e^{j\frac{2\pi d(N-1)}{\lambda}\sin(\theta_{\text{com}})} & e^{j\frac{2\pi d(N-1)}{\lambda}\sin(\theta_{\text{rad}})} \end{bmatrix}. \tag{8}$$

Considering then a TX architecture with full amplitude and digital control, similar to Arch.3, the transmitter beamforming weights can be expressed as

$$\mathbf{w}_{\text{tx}}^T = \begin{bmatrix} \sqrt{\rho} & \sqrt{1-\rho} \end{bmatrix} (\mathbf{A}_{\text{tx}}^H \mathbf{A}_{\text{tx}})^{-1} \mathbf{A}_{\text{tx}}^H, \tag{9}$$

where the parameter $\rho \in [0, 1]$ controls the power distribution between the communication and sensing beams and $(\cdot)^H$ denotes the Hermitian transpose [15]. The RX beamforming weights $\mathbf{w}_{\text{rx}}$ are similarly obtained by defining a matrix $\mathbf{A}_{\text{rx}}$ which only considers the steering vector corresponding to the sensing direction (θ_{rad}) and possibly a null in the communication direction (θ_{com}). Additional windowing can be applied to control the desired sidelobe level or the main beam width.

B. Proposed Joint Optimization Approach

However, the above separate design of the TX and RX beamformer will result into a considerable contribution of the communication beam in the CRP, defined in (7). This produces a high CRP gain at θ_{com} that degrades the overall radar performance, i.e., the ability to sense targets at other directions. This problem is illustrated in Fig. 2, which shows how the CRP of the reference beamforming solution is indeed sensitive to the echoes at the communications direction θ_{com}.

To overcome this challenge, we propose an optimization problem and approach to jointly design the TX and RX

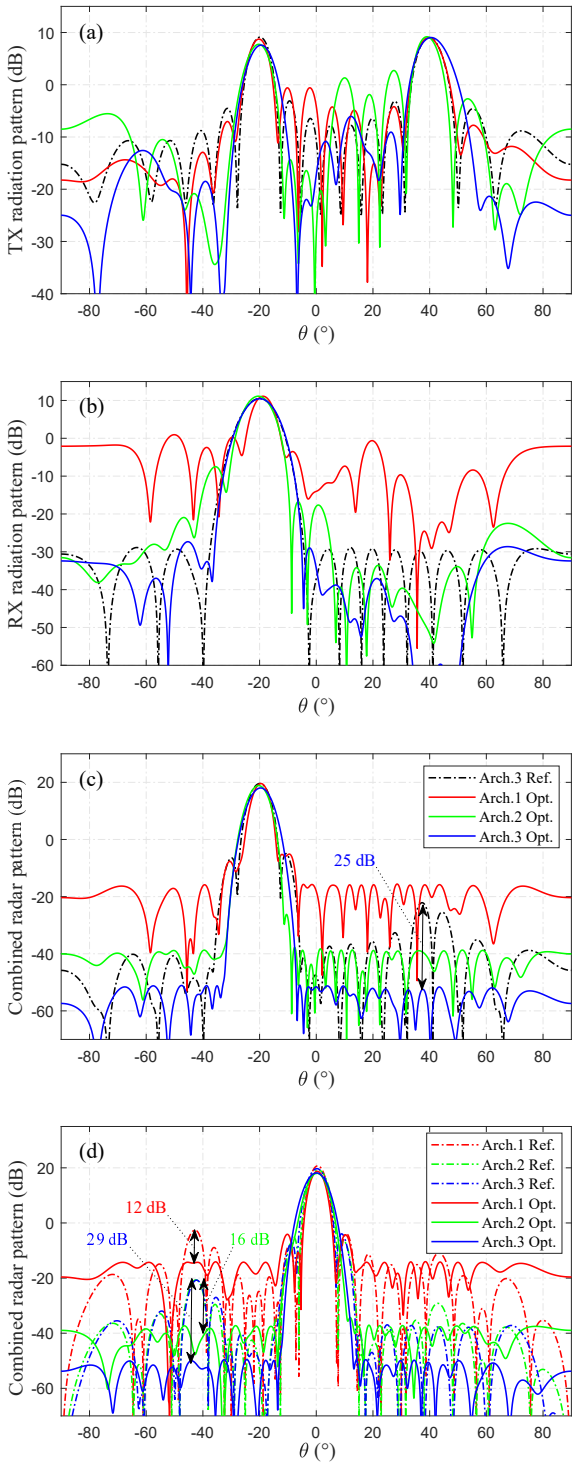

Fig. 2. Illustration of optimized (a) TX beam patterns, (b) RX beam patterns and (c) combined radar patterns with different array Architectures 1–3, for $\theta_{\text{com}} = 40°$ and $\theta_{\text{rad}} = -20°$, considering design parameters of $\Delta = 26°$, $G_{\text{com}} = 9$ dB and $G_{\text{rad}} = 18$ dB. Curves are as identified in the legend in (c). Also the corresponding patterns with reference solution and assuming Architecture 3 are shown. Similarly, (d) shows another example of the CRP for $\theta_{\text{com}} = -40°$ and $\theta_{\text{rad}} = 0°$ with the same design parameters. The gains obtained through the proposed optimization, to suppress an echo from θ_{com}, are also shown in (c) and (d).

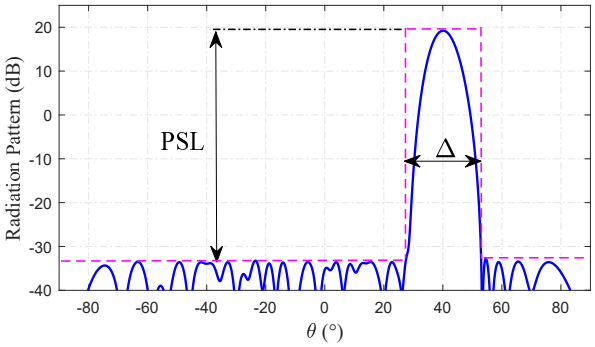

Fig. 3. Illustration of a combined radar pattern with directional radar beam at $\theta_{\text{rad}} = 40°$. The proposed beamformer optimization maximizes the peak sidelobe level PSL with Δ denoting the width of the main beam mask.

beamforming weights that minimize the negative effects of the TX communication beam in the overall radar performance. Specifically, the proposed optimization framework is defined as the following maximization problem, as

$$\max_{\boldsymbol{\alpha}_{\text{tx}},\boldsymbol{\beta}_{\text{tx}},\boldsymbol{\alpha}_{\text{rx}},\boldsymbol{\beta}_{\text{rx}}} PSL, \tag{10}$$

subject to

$$\|\boldsymbol{\alpha}_{\text{tx}}\|^2 = 1 \text{ and } \|\boldsymbol{\alpha}_{\text{rx}}\|^2 = 1, \tag{11a}$$
$$10\log_{10}(|F_{\text{tx}}(\theta_{\text{com}})|^2) \geq G_{\text{com}}, \tag{11b}$$
$$10\log_{10}(|R_{\text{rad}}(\theta_{\text{rad}})|^2) \geq G_{\text{rad}}, \tag{11c}$$
$$\alpha_{\text{tx},n} \geq 0 \text{ and } \alpha_{\text{rx},n} \geq 0, \tag{11d}$$
$$-\pi \leq \beta_{\text{tx},n} \leq \pi \text{ and } -\pi \leq \beta_{\text{rx},n} \leq \pi. \tag{11e}$$

where the peak sidelobe level (PSL) of the CRP reads

$$PSL = \frac{|R_{\text{rad}}(\theta_{\text{rad}})|^2}{\max_{\theta}\left(|R_{\text{rad}}(\theta)|^2\right)}, \tag{12}$$

while $\theta = [-90°, \theta_{\text{rad}} - \Delta/2] \cup [\theta_{\text{rad}} + \Delta/2, 90°]$ corresponds to a mask of width Δ around the radar beam θ_{rad}. Fig. 3 shows an illustrative example of the CRP and how the main parameters are defined in the optimization problem. As can be observed, we consider a constrained problem where the average normalized power constraints are set to one, in both the TX and RX sides with (11a). Additionally, the optimized TX beam pattern must provide a minimum antenna gain of G_{com} for the communications link at θ_{com}, imposed by (11b). Similarly, a minimum CRP gain of G_{rad} in the direction of the radar beam θ_{rad} is also set with the constraint in (11c). Finally, the parameter Δ allows to control the radar beam width and consequently the radar angular resolution.

IV. Numerical Results and Analysis

Numerical evaluations are next carried out to assess and demonstrate the performance of the joint beamforming optimization proposed in Section III, as well as to compare the different antenna array architectures and their feasibility for the JCAS operation. In the evaluations, ULA with $N = 16$ elements uniformly spaced at half the wavelength is considered and the network center-frequency is assumed to be $f_c = 28$ GHz.

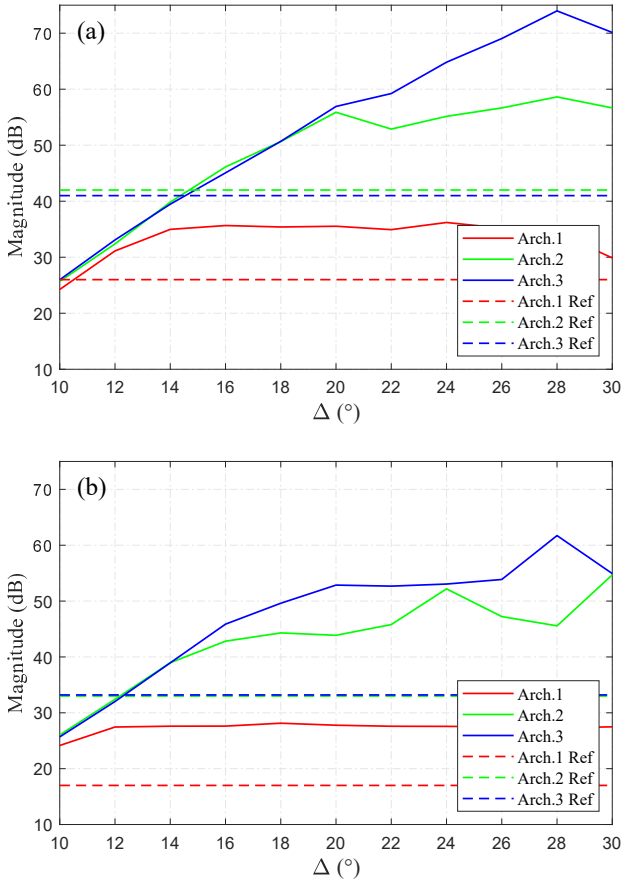

Fig. 4. Peak sidelobe level performance wrt. varying Δ for $\theta_{\text{com}} = 40°$ and $\theta_{\text{rad}} = -20°$ for optimized TX and RX weights with parameters (a) $G_{\text{com}} = 9$ dB and $G_{\text{rad}} = 18$ dB and (b) $G_{\text{com}} = 11.5$ dB and $G_{\text{rad}} = 9$ dB.

A. Obtained CRP and PSL Results

Concrete examples of the optimized radiation patterns are given in Fig. 2, illustrating the multibeam operation with communication and sensing beams at $\theta_{\text{com}} = 40°$ and $\theta_{\text{rad}} = -20°$, respectively. In this case, given the array size of $N = 16$, a maximum nominal gain of $10\log_{10}(N) = 12$ dB can be achieved. In the beamforming design, we consider a minimum TX antenna gain at θ_{com} to be $G_{\text{com}} = 9$ dB, implying thus a penalty of 3dB with respect to the maximum achievable gain (which would mean single-beam configuration). The rest of the design parameters are set as $\Delta = 26°$ and $G_{\text{rad}} = 18$ dB. The performances of the proposed optimization under the three different architectures (Arch. 1 – Arch. 3) are compared with the reference case which considers separate design of the TX and RX beamforming weights while allowing full amplitude and phase control (Arch. 3). In the reference case, the TX is designed to provide two beams with same gain of 9 dB, while the RX provides a single beam in the sensing direction and simultaneously suppresses sidelobes in the rest of the directions by applying a Hamming window.

Fig. 2c) presents the obtained CRPs for the different architectures. As can be observed, the Arch.3 which provides more flexibility in the beamforming design, shows the best performance in terms of mitigation of possible interferences with a peak sidelobe level of around 70 dB. Using more constrained architectures, suppressions of 35 dB and 60 dB are achieved with Architectures 1 and 2, respectively. The results also clearly show that when considering Arch.3, the proposed optimization achieves a sidelobe suppression improvement of 25 dB compared to the reference case, demonstrating the novelty of the proposed method. This considerable improvement can only be achieved when the TX and RX beamforming weights are jointly optimized, and permits to precisely null the TX communication beam and the strong sidelobes in the RX radiation pattern as shown in Fig. 2b).

In addition, we analyze the effect of the parameter Δ in the beamforming optimization in two different cases, namely when the penalty at the communication beam gain is 1) 3 dB ($G_{\text{com}} = 9$ dB) and 2) only 0.5 dB ($G_{\text{com}} = 11.5$ dB). As can be observed through the obtained results shown in Fig. 4, the parameter Δ controls the radar beam width and consequently the peak sidelobe level of the CRP. Increasing this parameter improves the peak sidelobe level, however, it also degrades the radar angular resolution. Similar to the results shown in Fig. 2, Arch.3 facilitates better performance compared to the other two architectures. It can also be observed that better sidelobe suppression is achieved when the magnitudes of the TX communication and sensing beams are similar, evidenced in Fig. 4a). Fig. 4 also shows the PSL behavior for the reference cases where the TX and RX beamformers are designed separately, demonstrating that large PSL improvements are available when the proposed joint optimization based beamformers are adopted.

Finally, we address and analyze the trade-off between the communication and radar performance in terms of the optimization parameters for a fixed communication beam at $\theta_{\text{com}} = 40°$, while the JCAS system scans angles between -60° to 60° with steps of 2° and adopting the Arch.3. Fig. 5a) shows the achieved CRP and TX communication gains in terms of the different optimization parameters. It can be observed that the CRP gain is limited depending on the chosen communication penalty G_{com}. Additionally, in the special case when both communication and radar beams are aimed to the same direction, the optimization algorithm provides a single beam with maximum gain for both TX and CRP patterns. Fig. 5b) presents then the PSL performance for different sensing directions. It is noted that the performance of the proposed optimization algorithm depends on the directions of the beams. Specifically, at larger sensing angles with respect to the normal of the array (e.g. -60° and 60°), the radiation patterns are more difficult to optimize and therefore the PSL performance is degraded to certain extent.

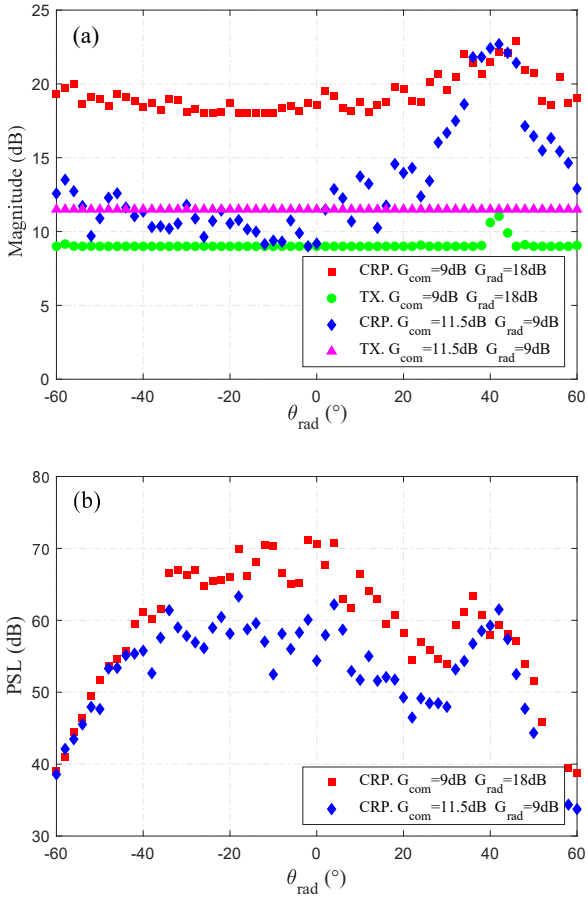

Fig. 5. (a) Trade-off between the communication and radar performance and (b) PSL for fixed $\theta_{\text{com}} = 40°$ while varying θ_{rad} under two different optimization parameters.

B. Obtained Sensing Results

We next present further numerical results to validate and assess the actual sensing performance of the proposed beamforming optimization approach in a practical scattering environment with 15 static targets of point source nature, illustrated in Fig. 6a). Five of these targets are deliberately placed in the direction of the communication link, at $\theta_{\text{com}} = 40°$, with a radar cross section (RCS) of 10 m^2. The rest of the targets are uniformly distributed in the sensed area at distances within 10 to 25 m and angles from -40 to 40°, with RCS of 1 m^2. The gNB transmission power is +30 dBm and the total thermal noise in the receiver is -88 dBm. The JCAS system has again a fixed communication beam towards the UE while the sensing beam scans the angles between -60 to 60° with a step of 1°. Furthermore, the sensing beam time resolution is ca. 0.08 ms meaning that the gNB transmits for each multibeam case a 5G NR waveform of 10 OFDM symbols with carrier bandwidth of 400 MHz and subcarrier spacing of 120 kHz [7]. According to these specifications, the complete sensing sweep lasts for ca. 10 ms. For the radar processing, we adopt subcarrier-domain processing, utilizing directly the transmit and receive subcarrier samples similar to [6], [12], including coherent integration of different range profiles.

First, in Fig. 6b) and Fig. 6c), we illustrate the sensing capabilities when the TX is designed to provide two beams with the same gain, while the RX provides a single beam

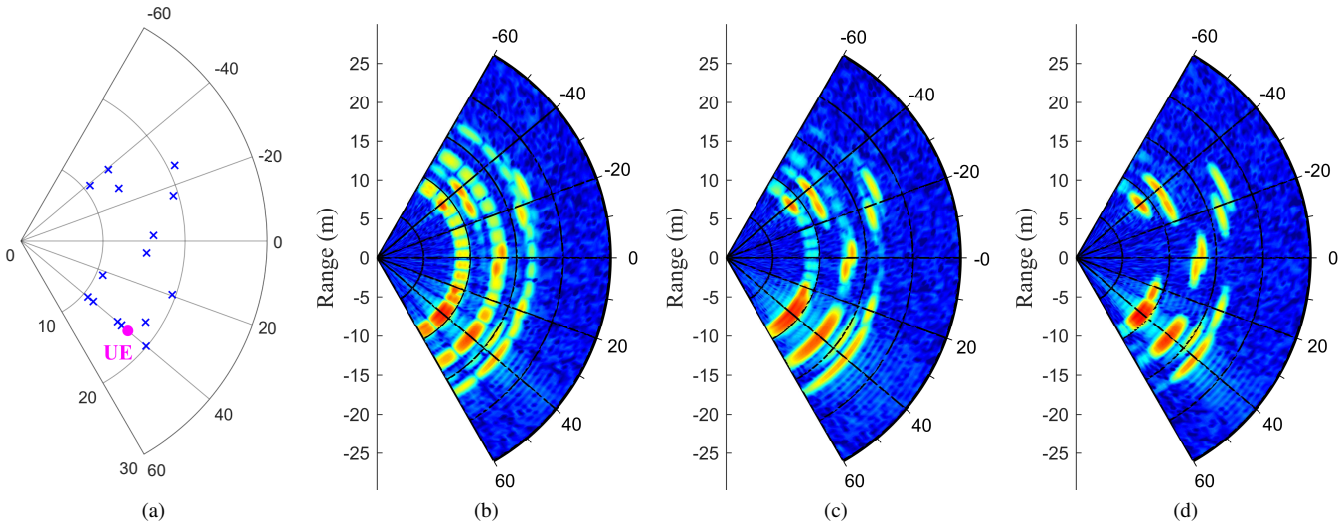

Fig. 6. (a) Considered scattering scenario with 15 targets and user equipment (UE) at $\theta_{\text{com}} = 40°$. Radar images for reference separate TX and RX beamforming design, without and with sidelobe suppression in (b) and (c), respectively. In (d), the radar image is shown with the proposed jointly optimized TX and RX beamformers for $\Delta = 26°$, $G_{\text{com}} = 9$ dB and $G_{\text{rad}} = 18$ dB.

in the sensing direction without or with sidelobe suppression, essentially reflecting the reference solution. It can be clearly observed that the communication beam interference generates strong sidelobes, which produce a substantial masking effect along the rest of the sensing directions, which can potentially mask weak targets. In contrast, by applying the proposed optimization based beamforming design, the sidelobe levels can be largely suppressed allowing thus to avoid such masking problem. Fig. 6d) presents the corresponding radar image when the jointly optimized beamformer is used with parameters $\Delta = 26°$, $G_{\text{com}} = 9$ dB and $G_{\text{rad}} = 18$ dB. As can be observed, the radar image is largely improved compared to those obtained through the reference method.

V. Conclusion

In this paper, RF beamformer optimization for joint communications and radar operation in millimeter-wave 5G NR networks was addressed. In the considered system, multibeam TX beamforming is adopted such that one beam is utilized for the communications link while the other beam is simultaneously used for sensing, and the radar RX beamformer is essentially matched to the sensing beam. In order to reduce the impact of the echoes due to the communications beam, that essentially act as interference, beamformer optimization problem was then formulated, where the TX and RX beamforming weights are jointly optimized to maximize the radar performance, while considering the communications link and selected implementation issues as constraints. Numerical results demonstrated that a considerable sensing performance improvement can be achieved by the proposed optimized multibeam technique in comparison with the existing reference methods. Moreover, the paper shows and demonstrates that clear sensing performance improvements are available at the cost of a very minor SNR penalty in the communications link, given that beamformer optimization is properly executed.

References

[1] B. Paul, A. R. Chiriyath, and D. W. Bliss, "Survey of RF communications and sensing convergence research," *IEEE Access*, vol. 5, pp. 252–270, 2017.

[2] G. C. Tavik *et al.*, "The advanced multifunction RF concept," *IEEE Trans. Microw. Theory Tech.*, vol. 53, no. 3, pp. 1009–1020, Mar. 2005.

[3] M. L. Rahman, J. A. Zhang, X. Huang, Y. J. Guo, and R. W. Heath Jr, "Framework for a perceptive mobile network using joint communication and radar sensing," *IEEE Trans. Aerosp. Electron. Syst.*, pp. 1–1, 2019.

[4] F. Liu, C. Masouros, A. Petropulu, H. Griffiths, and L. Hanzo, "Joint radar and communication design: Applications, state-of-the-art, and the road ahead," *CoRR*, 2019, available at: https://arxiv.org/abs/1906.00789.

[5] M. Alloulah and H. Huang, "Future millimeter-wave indoor systems: A blueprint for joint communication and sensing," *Computer*, vol. 52, no. 7, pp. 16–24, Jul. 2019.

[6] M. Braun, "OFDM radar algorithms in mobile communication networks," Ph.D. dissertation, Karlsruhe Institute of Technology, 2014.

[7] "3GPP TS 38.104 v15.4.0, "NR; Base Station (BS) radio transmission and reception", Tech. Spec. Group Radio Access Network, Rel. 15," Dec. 2018.

[8] P. Kumari, M. E. Eltayeb, and R. W. Heath, "Sparsity-aware adaptive beamforming design for IEEE 802.11ad-based joint communication-radar," in *RadarConf18*, Apr. 2018, pp. 0923–0928.

[9] M. Kiviranta, I. Moilanen, and J. Roivainen, "5G radar: Scenarios, numerology and simulations," in *ICMCIS*, May. 2019, pp. 1–6.

[10] P. Kumari *et al.*, "IEEE 802.11ad-based radar: An approach to joint vehicular communication-radar system," *IEEE Trans. Veh. Technol.*, vol. 67, no. 4, pp. 3012–3027, Apr. 2018.

[11] J. A. Zhang, X. Huang, Y. J. Guo, J. Yuan, and R. W. Heath, "Multibeam for joint communication and radar sensing using steerable analog antenna arrays," *IEEE Trans. Veh. Technol.*, vol. 68, no. 1, pp. 671–685, Jan. 2019.

[12] C. Baquero Barneto, T. Riihonen, M. Turunen, L. Anttila, M. Fleischer, K. Stadius, J. Ryynänen, and M. Valkama, "Full-duplex OFDM radar with LTE and 5G NR waveforms: Challenges, solutions, and measurements," *IEEE Trans. Microw. Theory Tech.*, vol. 67, no. 10, pp. 4042–4054, Oct. 2019.

[13] M. Richards, W. Holm, and J. Scheer, *Principles of Modern Radar: Basic Principles*. Institution of Engineering and Technology, 2010.

[14] R. W. Heath *et al.*, "An overview of signal processing techniques for millimeter wave MIMO systems," *IEEE J. Sel. Topics Signal Process.*, vol. 10, no. 3, pp. 436–453, Apr. 2016.

[15] S. Kutty and D. Sen, "Beamforming for millimeter wave communications: An inclusive survey," *IEEE Communications Surveys Tutorials*, vol. 18, no. 2, pp. 949–973, Secondquarter 2016.